Photonic Crystal Devices for Wavelength-Division-Multiplexing and Optical Modulation

Wei Jiang[*a,b], Yongqiang Jiang[a], Lanlan Gu[a], Xiaonan Chen[a], and Ray T. Chen[a]
[a]Microelectronics Research Center and Department of Electrical and Computer Engineering, the University of Texas, Austin, Texas 78758
[b]Omega Optics, 10435 Burnet Road, Suite 108, Austin, Texas 78758

ABSTRACT

This paper reviews photonic crystal (PC) based demultiplexers, and briefly reports our latest experimental achievement in ultra-compact, power-efficient silicon photonic crystal waveguide (PCW) modulators. We review the modeling techniques for photonic crystal superprism devices, which utilize anomalous refraction on a photonic crystal surface for wavelength demultiplexing. The finite difference time domain method tends to be time consuming for the superprism devices as such devices demand fine spatial grids to resolve fine wavelength difference. Other theoretical methods suffer a variety of other drawbacks. A general, efficient PC refraction theory that can handle any surface orientation is needed for scientific research and device design. We review a rigorous PC refraction theory that we recently developed for these needs. Essentially, the refraction problem can be rigorously solved by computing the electromagnetic field in only a single cell on the surface. A new concept, surface-orientation-dependent eigenmode degeneracy, is introduced to explain certain subtle effect that occurs when the surface orientation undergoes a slight change. In addition, the transmission of a Gaussian beam or other realistic beam profiles is discussed. A complete theoretical framework of the photonic crystal refraction and transmission has thus been established. The theory has been applied to design a high channel-count dense WDM demultiplexer with 3dB or lower losses. Lastly, a silicon PCW Mach-Zehnder modulator with an 80-micron interaction length is reported. The slow group velocity in PCWs is exploited to enhance the modulation efficiency and reduce the peak drive current to 0.15mA at a modulation depth over 90%.

Keywords: photonic crystal, superprism effect, modulator, refraction, wavelength division multiplexing, nanophotonics, Mach-Zehnder, dispersion surface, energy conservation, beam width

1. INTRODUCTION

The explosive growth of the Internet in the ending decade of last century has transformed almost all aspects of the society and our life. Accompanying the Internet marvel was an unprecedented demand of communication bandwidth, which was fortunately echoed by an emerging fiber-optic communications technology: wavelength division multiplexing (WDM). The wavelength-division-multiplexing technology has played a revolutionary role in expanding the bandwidth toward terabit communications. The transparent spectral windows of optical fibers are divided into small pieces called channels, each of which transmits signals undisturbed by others. This approach exploits the bandwidth of optical fibers to its ultimacy. A typical dense WDM (DWDM) network is enabled by important devices such as multiplexers (Mux), demultiplexers (DeMux) and optical add-drop multiplexers (OADM).

In the meantime, photonic crystals gradually entered the center stage of nanophotonics research. Photonic crystals (PCs) are a new class of artificial optical materials with periodic dielectric structures,[1,2] which result in unusual optical properties and unfold new dimensions for innovations in the photonics technology. Ideally, photonic crystals can be viewed as a composite of a periodic array of macroscopic low- or high-dielectric scatterers in a homogeneous high- or low-dielectric matrix, respectively. A real example is a single slab of semiconductor (high-dielectric) containing a periodic array of air-holes (low-dielectric), which forms a two-dimensional (2D) photonic crystal. The underpinning physics of photonic crystals emanates from early work by Yablonovitch[1] and John.[2] In a semiconductor, the periodic lattice of atoms causes electrons to have energy bands and energy gaps; in a photonic crystal, the periodic dielectric

* email: jiang@ece.utexas.edu

Active and Passive Optical Components for WDM Communications V, edited by Achyut K. Dutta, Yasutake Ohishi, Niloy K. Dutta, Jesper Moerk, Proc. of SPIE Vol. 6014, 60140F, (2005) · 0277-786X/05/$15 · doi: 10.1117/12.637281

lattice causes photons to have frequency bands and frequency gaps, the latter often being called *photonic band gap*(PBG). If the frequency of light (or photon) falls inside a PBG, the photonic crystal will reflect the light totally regardless of its incident angle. This is completely different from traditional dielectric media where light is totally reflected only for certain range of incident angles. This effect provides a superb optical confinement and wave-guiding mechanism unattainable through the conventional index-guiding scheme, which leads to a proliferation of studies in photonic crystal cavities and waveguides.[3-7] Another interesting physical concept is the equi-frequency (or iso-frequency) surface of a photonic crystal,[8-15] which is an analogy of the Fermi surface for an atomic crystal. In the case of an atomic crystal, the constant-energy surface in the reciprocal space can be drawn once the energy bands and bandgaps of electrons and the temperature are known; in the case of a photonic crystal, however, the equi-frequency surface is determined by the photonic band structures and the wavelength of the light source in use rather than the temperature. This gives ample freedom in exploring all parts of the equi-frequency surface as it is more convenient to vary the wavelength compared to varying the temperature for real-world applications. In the literature, the equi-frequency surface is more often named the *dispersion surface*. Sometimes it is also called iso-frequency surface as illustrated in Fig. 1(a).[12]

Anomalous refraction of light at an interface between a photonic crystal and a homogeneous medium has been studied recently.[8-14] The refraction angle was found to be sensitive to the incident angle and wavelength in certain cases.[8] A prism made up of a photonic crystal would have a dispersion capability 500 times stronger than a prism made of a conventional medium.[9] These phenomena were called "superprism" effect accordingly, and were proposed to be utilized for wavelength-division-multiplexing (WDM)[8-10] and superlens[11] applications. Fundamentally, these phenomena arise from the high anisotropy of the dispersion surface of a photonic crystal. As we shall see, the dispersion surface of an isotropic medium must be a sphere; the dispersion surface of a homogeneous anisotropic medium such as a conventional birefringent crystal is an ellipsoid; whereas the dispersion surface of a photonic crystal consisting of two isotropic materials could be highly complex and have multiple branches. In Fig. 1(a), the dispersion surface has a star-like shape.

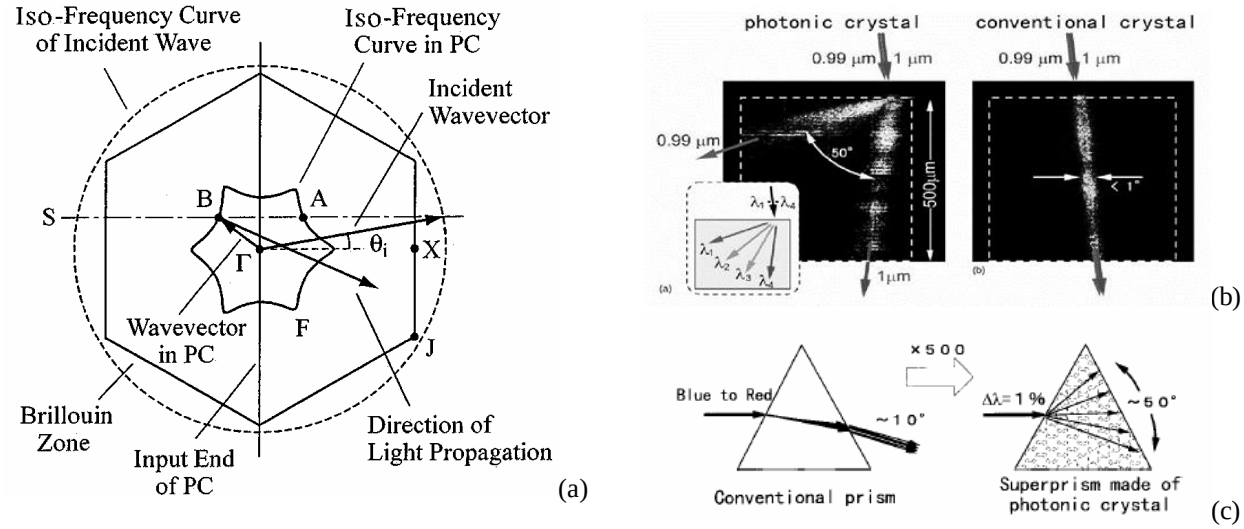

Figure 1 (a) Dispersion surface (iso-frequency curve) of a photonic crystal, from Ref. [12]. (b) Wavelength-sensitive refraction—superprism effect, from Ref. [8]. (c) Illustration of the *superprism* concept, from Ref. [9]

In past few years, we have conducted research to employ photonic crystal cavities and waveguides to make optical add-drop multiplexers,[6-7] and studied the superprism effect for WDM demultiplexer applications.[14-15] In this paper, we will review the latter part of our work.

2. PAST WORK IN THE SUPERPRISM EFFECT AND DEMULTIPLEXER DESIGN

Compared to the extensive work in photonic crystal lasers and waveguides, research on the superprism effect has not received widespread attention since Kosaka et al. first discovered the effect although recent surge of interest in negative

refraction overlaps with the superprism research to certain extent. One major stumbling block lies in the modeling technique for the superprism effect. A variety of theoretical methods are available to model light refraction and propagation in photonic crystals, including transfer matrix method,[16-18] the scattering theory of dielectric sphere lattices[19-21] or the multiple scattering method,[22] the internal field expansion method,[23] and the popular Finite Difference Time Domain techniques.[12,24] Note some of these methods could have a number of flavors. For example, the transfer matrix method can be based on planar waves or spherical waves. So far, none of them has successfully produced a demultiplexer design of practical value in terms of optical loss and wavelength spacing. However, some interesting structures have been proposed that could pave the way toward the realization of a photonic crystal demultiplexer. In the upper left panel of Fig. 2, light impinges on a photonic crystal segment that exhibits the superprism effect, different wavelengths refracted in different directions, each reaching a distinct output waveguide.[24] A noteworthy feature of this structure is the integration of the photonic crystal superprism and the photonic crystal waveguides. However, the four wavelengths used in this simulation have a minimum spacing of 5%, which is over 100 times higher than the wavelength spacing required for DWDM applications. Baba et al. explored device geometries beyond surface-parallel slabs.[12] In the upper right panel of Fig. 2, a structure with beveled output edges is presented. The other three pictures on this panel illustrate the field intensity for different wavelengths simulated by the FDTD technique.[12] An important idea that that paper attempted to demonstrate through these structures was to use gratings to flatten the output edge and suppress diffraction and divergence of the output beam.[12] As seen in the FDTD simulated optical field patterns, the diffraction suppression was good in some, but not all, cases. In the lower left panel of Fig. 2, a semi-circular superprism device actually made in Krauss' group in UK is displayed.[10]

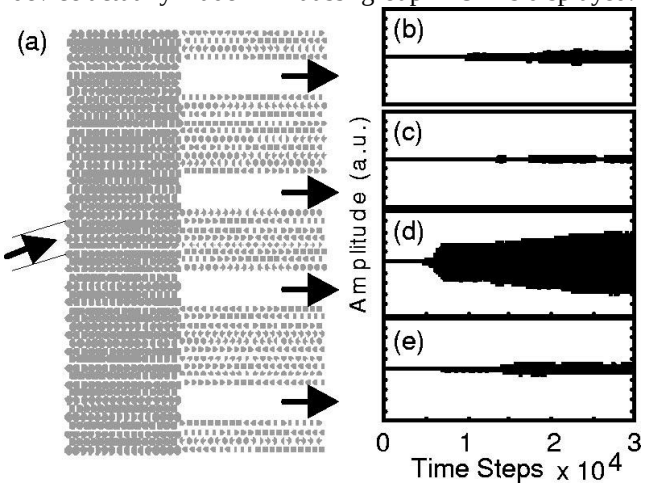

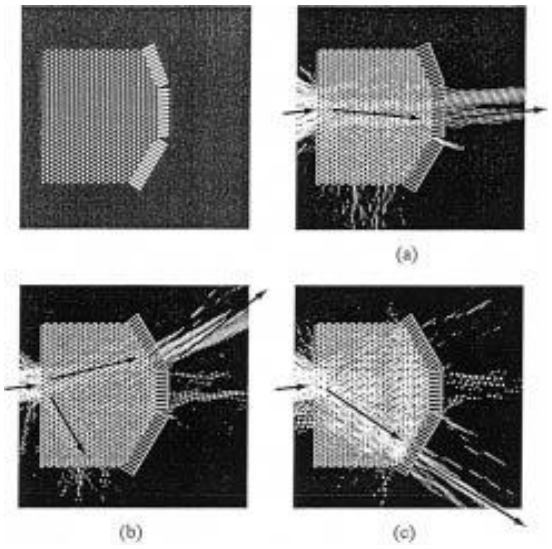

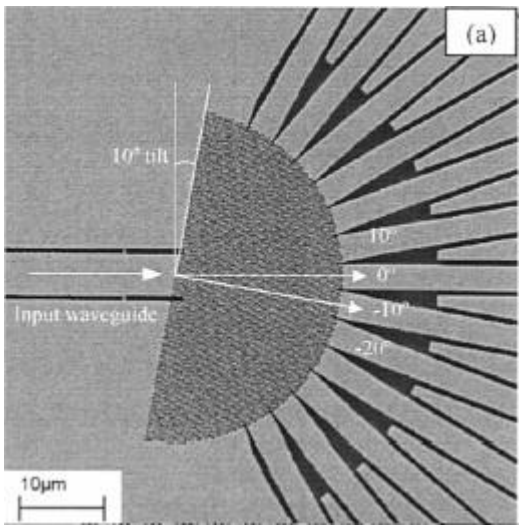

Figure 2 Various superprism devices.
Upper-left panel: A 4-channel demultiplexer; the simulation shows at one frequency, significant intensity is present in the third waveguide from the top (Ref. 24).
Upper-right panel: Non-slab geometry and grating flatten output surface (Ref. [12]).
Lower-right panel: Semi-circular photonic crystal segment, where an input waveguide guides light in from the left and multiple output waveguides collects light in the radial direction on the right (Ref. [10])

Based on the effective size of real-space computational domain, all of the methods for photonic crystal transmission can be divided into three categories, as tabulated in Fig. 3(a). The first category can be named the whole-space method,[22,24] which calculates the optical field (electric and/or magnetic field) in the whole space (or in the whole photonic crystal). The second category can be named the one-dimensional (1D) supercell methods,[23] which calculates the field in only a supercell of the photonic crystal to solve the transmission problem. This method appears to be applicable to a photonic crystal slab only. The last category is the single-cell method,[18] which calculates the field in a single cell per surface and solves the refraction problem surface by surface. Some methods can be in more than one categories, depending on the detailed implementation. Generally, the last category of methods are most efficient and versatile in practical designs. A detailed comparison of the numerical advantages of these methods is beyond the scope of this paper.

Here, we shall further discuss two particular approaches of the photonic crystal transmission problem. It is our perception that the Finite Difference Time Domain (FDTD) method[12,24] is the most popular numerical approach employed in practice. This is evidently attributed to the wide applicability of FDTD algorithm, the wide availability of the FDTD software with an easy-to-use graphic interface for computer-aided design. However, FDTD simulations can be inefficient in studying photonic crystal refraction. Essentially, *refraction is a phenomenon localized at the interface between two media*, as shown in Fig. 3(b). However, in FDTD simulations, one often needs to use a large enough space to enclose the whole photonic crystal, and calculates the field inside the whole computational domain to solve the problem, as illustrated in Fig. 1(b). When the photonic crystal is large enough, such an approach becomes extremely inefficient. On the other hand, when the photonic crystal is small enough such that the surface evanescent waves dominate over the propagating waves inside the *whole* photonic crystal,[25] FDTD simulations can be a good approach to the problem. However, when such a case occurs, the "photonic crystal" has almost lost its bulk properties and there might be no advantage of considering such a fragment of photonic nano-structure from the perspective of photonic crystals. This reminds us the size effect in other materials.[26] Exploring the limit when the size of a photonic crystal is too small to be a crystal meaningfully is an interesting question.

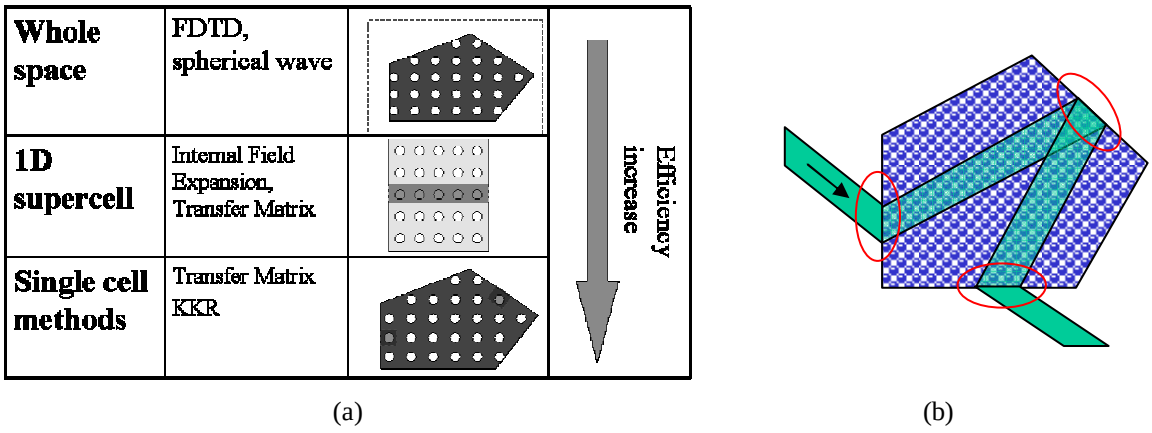

Figure 3 Comparison of various computational methods for photonic crystal transmission, refraction, and reflection (from Ref. [14]) (a) Three categories of methods, classified by the size of real-space computational domain. (b) Refraction is an effect localized at the surfaces as indicated, whereas the whole space methods must calculate the field in every cell of the photonic crystal to determine the transmission amplitudes along the light path. It is desirable that the photonic crystal refraction problem can be solved on the surface in the same fashion we apply Snell's law to a homogeneous medium.

The transfer matrix method is another method widely employed by researchers. For more than two decades, this method has been extensively studied for diffraction gratings, and many flavors of this method have been developed.[27,28] Essentially, it uses a matrix to relate the electromagnetic field on the front and back surfaces of a photonic crystal slab, and this matrix is called the transfer matrix. Typically, the transfer matrix method needs to stratify a 2D or 3D photonic crystal slab into many slices. The transfer matrix of the whole slab equals the product of the transfer matrix of each slice. If each slice consists of a complete layer of photonic "atoms," then one may further slice it into many thinner layers, each of which can be regarded homogeneous along the depth direction. Then a plane wave based method can be

employed to compute the transfer matrix across each slice.[18] Some spherical-wave approaches can directly compute the transfer matrix of each layer of photonic atoms if the atoms are spherical in shape.[19-21] There are yet other more sophisticated methods. Nonetheless it is our understanding that the plane-wave based "atom"-slicing approach is easiest to understand and implement, and versatile in treating various types of scatterer geometric shapes or spatial dielectric functions. Regardless of the approach, the transfer matrix method generally calculates the eigenvalues $\exp(ik_y d)$, where k_y is the wavevector component normal to the surface and d is certain distance normal to the surface. As we know, some k_y are real, but the others are complex. When complex k_y's appear on the exponent, the eigenvalues $\exp(ik_y d)$ will spread over a larger scale in value due to the nature of the exponential function. Some of the eigenvalues $\exp(ik_y d)$ having small magnitudes could be difficult to compute accurately.

In addition, in the scattering matrix approach commonly employed to stabilize the computation, the number of matrix inversion and multiplication operations grows linearly with the number of layers/slices.[27] It would be preferred that one can find the eigenvalues k_y directly rather than through the exponential form. Also it would be desirable that we can avoid complicated numerical procedures such as matrix inversion in the computation.

3. A NEW REFRACTION THEORY

As we have seen in the preceding section, to design photonic crystal based demultiplexers requires a refraction theory (1) that works for arbitrary surface orientation, (2) that does not demand formidable computation resources in proportion to the size of a photonic crystal superprism, and (3) that can resolve the refraction of two closely spaced wavelengths.

In this part, we will present a theory that satisfies all these requirements, which leads to the first viable 2D superprism demultiplexer design.[15] The theory itself involves a significant amount of mathematics, including the topology theory. In the appendix, we will summarize the major findings of our theory in two theorems. In this part, however, we will give a narrative of the framework of the theory, which facilitates the understanding of the demultiplexer design presented at the end.

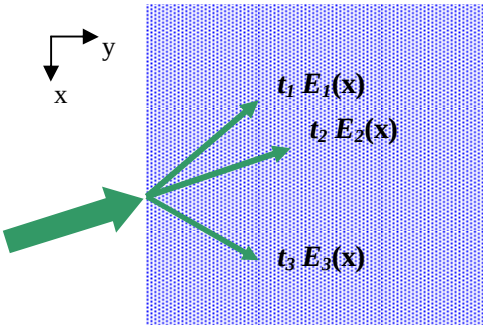

Figure 4 Single interface problem: a light beam impinges on the surface of a semi-infinite photonic crystal. Multiple propagating modes may be excited. The *x*-axis is parallel to the surface, where y-axis is perpendicular to the surface. Unless otherwise indicated, it is implied that the origin of the coordinate system is located on the surface

Mathematically, the refraction problem is essentially a semi-infinite problem as shown in Fig. 4. Unlike conventional dielectric media, a large number of refracted beams can be excited in the semi-infinite photonic crystal region. Each of these beams corresponds to a propagating mode, $\boldsymbol{E}_i(\mathbf{x})$, of the photonic crystal. Here $\boldsymbol{E}_i(\mathbf{x})$ represents the electric field of a given mode; equivalently, one may use the magnetic field $\boldsymbol{H}_i(\mathbf{x})$ to represent a mode. To find the coupling amplitude t_i of each excited propagating mode, the refraction problem must be solved. The basic steps of our theory are illustrated in Fig. 5. First, starting with the Maxwell's equations, one needs to solve for the eigenmodes of the semi-infinite photonic crystal. For simplicity, we shall consider the TM polarization (magnetic field in plane) in 2D space in the following discussions, although all conclusions can be readily generalized to any 3D case. Generally, the Maxwell's equations can be converted into a second order partial differential equation, which has a handy form for the 2D TM case

$$\nabla^2 E(\mathbf{x}) + \omega^2 \varepsilon(\mathbf{x}) E(\mathbf{x}) = 0 . \quad (1)$$

The spatially varying dielectric constant $\varepsilon(\mathbf{x}) = \sum_{\mathbf{G}} \varepsilon(\mathbf{G}) \exp(i\mathbf{G}\cdot\mathbf{x})$, where $\mathbf{G}$ is a reciprocal lattice vector; and

$$E(\mathbf{x}) = \exp(i\mathbf{k}\cdot\mathbf{x}) \sum_{\mathbf{G}} E(\mathbf{G}) \exp(i\mathbf{G}\cdot\mathbf{x}) , \quad (2)$$

according to the Bloch theorem. Equation (1) can now be written as

$$-[(k_x+G_x)^2+(k_y+G_y)^2]E(\mathbf{G})+\omega^2\sum_{\mathbf{G}'}\varepsilon(\mathbf{G}-\mathbf{G}')E(\mathbf{G}')=0. \qquad (3)$$

This is the same equation used to calculate the photonic bands and bandgaps for a bulk photonic crystal. For the photonic band calculations for a bulk (infinite spatial extent) photonic crystal, we are given all the components of the wavevector k_x, k_y (including k_z in a 3D case), and we need to solve for eigenvalues of frequency ω. On the other hand, for a refraction problem—consider a real refraction experiment—we know the wavelength of incident wave (assume monochromatic) and we know the incident angle. From these, effectively, we know the frequency ω, and the surface tangential component k_x; and our goal for the refraction problem becomes to solve for the surface normal component k_y in the semi-infinite photonic crystal. This marks a major difference between the photonic band calculation for a bulk (infinite) photonic crystal and the refraction problem for a semi-infinite photonic crystal. Mathematically, the set of linear equations in Eq. (3) can be converted into a matrix form. Then the two problems have the following matrix forms.

$$\text{Band calculation (infinity photonic crystal):} \quad [A']E-\omega^2[B']E=0, \text{ or } [A'']E=\omega^2E, \qquad (4a)$$

$$\text{Refraction problem (semi-infinite crystal):} \quad ([A]k_y^2+[B]k_y+[C])E=0. \qquad (4b)$$

Here E is a column vector whose elements are $E(\mathbf{G})$. The square matrices [A'], [B'], and [A"] are related by

$$[A'']=[B']^{-1}[A']$$

are square matrices whose elements depend on k_x and k_y, On the other hand, the square matrices [A], [B] and [C] depend on k_x and ω. The mathematical form of the refraction problem may look unfamiliar for physics and engineering researchers. It is called a quadratic eigenvalue problem, which can be readily converted, through some standard procedures,[29,30] into a regular eigenvalue problem. Then the eigenvalue solution part of the refraction problem can be handled with general-purpose matrix eigenvalue algorithms. Although not difficult, we shall refrain from elaborating the details further. Note that although both Eq. (4a) and Eq. (4b) are just Eq. (3) rewritten in different ways, the sets of eigenmodes obtained from them are not identical. The eigenmodes solved from Eq. (4a) are purely propagating modes with real k_x and k_y values, whereas the eigenmodes for the refraction problem Eq. (4b) can contain non-propagating modes with complex values of k_y (even if k_x and ω are both real). These correspond to modes that either decay spatially in the semi-infinite photonic crystal, or exponentially grow in the semi-infinite photonic crystal.

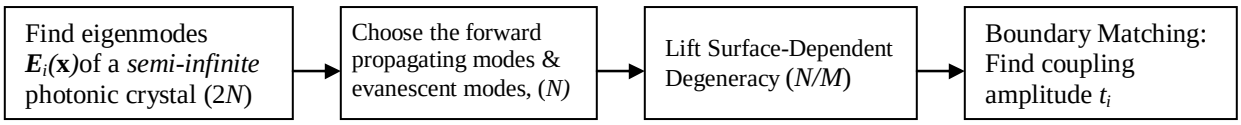

Figure 5 procedures for solving the refraction problem for a planar incident wave

Up to this point, we have completed the first step in Fig. 5. However, as we have noticed, that there are some eigenmodes not physically meaningful in the solved eigenmodes. The modes can not exponentially grow as it extends deep into the semi-infinite photonic crystal. Furthermore, among the propagating modes, there are forward propagating modes whose energy flow points into the semi-infinite photonic crystal (called "up modes" in Ref. 15), whereas other modes has their Poynting vectors pointing backward (called "down modes" in Ref. 15). The latter are not physically meaningful if the light is incident from outside the photonic crystal and should not be used in matching the boundary conditions. It can be shown that among the solved eigenmodes with real k_y values, there are always equal number of forward propagating modes and backward propagating modes. And among the non-propagating modes, the evanescent modes and the exponential growth modes also appear in pairs. Therefore, among 2N solved eigenmodes, there are N modes that can be physically excited by a planar wave incident from the y<0 side. Now we have completed the second step illustrated in Fig. 5. This step is summarized as Theorem 1 in the Appendix.

Furthermore, some solved eigenvalues k_y that remain after the preceding elimination procedure are located far outside the first Brillouin zone (BZ). A simplistic approach would be to eliminate those modes with $\mathbf{k}=(k_x,k_y)$ outside the first BZ—note that the value of k_x is given for a refraction problem. However, this would only work for simple lattice types and trivial surface orientations such as the (10) surface of a square lattice. Here the surface orientation is given in the form of two Miller indices (hk) for a 2D lattice, and (10) surface is a 2D analogue of the (100) surface of a 3D cubic

lattice. For surfaces like (*hk*)=(23) or indexed by larger integer values, the basis vectors of the lattice needs to be redefined to reflect the surface orientation. It can be shown that only a 1D Brillouin zone could remain for a semi-infinite photonic crystal due to broken translational symmetry. More details will be discussed in the Appendix or one may refer to Ref. 15. The k_y eigenvalues must be restricted to one of the 1D Brillouin zones. It can be readily proved that for a Fourier expansion that has includes M components in the surface normal direction, all eigenvalues of k_y outside such a 1D Brillouin zone give M replicas of those inside. To remove such degeneracy, one must restrict to those modes inside one 1D Brillouin zone. Therefore, the number of modes will be reduced to N/M. Numerically, it is always preferred to choose the first 1D BZ that is centered around k_y=0 for best numerical accuracy.

On the contrary, there exist quasi-periodic surfaces[31] whose orientation can be effectively described by irrational numbers (*hk*). In these cases, the semi-infinite photonic crystal does not have any translational symmetry. Note these quasi-periodic surfaces are not artificially fabricated by tiling as in the case of Penrose lattice,[32] instead, they are made by precisely cutting a regular photonic crystal in a specific orientation. In such cases, there is no eigenmode degeneracy, and the reduction of modes by M is not applicable to this case. For the transition between periodic and quasi-periodic surface orientations, we predicted that a slight variation of surface orientation that changes a surface from periodic to quasi-periodic would cause one refracted beam to split into essentially infinite number of beams. The underpinning physical principle for this effect is explained in detail in Refs. 15 & 33 and is discussed in the Appendix.

Now that we have completed the third step, we are ready to solve the boundary conditions. Essentially, we need to solve a set of linear equations to find the amplitude t_i for each eigenmode E_i. For the coordinate system displayed in Fig. 4, the boundary conditions are formulated as matching the amplitudes of surface wave components $\exp[ip_x(\mathbf{G})x]$, where

$$p_x(\mathbf{G}) = q_{0x} + G_x, \qquad (5)$$

Here q_{0x} is the x component of incident wave vector $\mathbf{q}_0$, and $\mathbf{G}$ runs over all reciprocal lattice vectors. It can be readily shown that for an ordinary surface that can be described by integer Miller indices, the values of p_x are identical for a set of reciprocal lattice vectors whose G_x values are the same. On the other hand, for a quasi-periodic lattice, no two reciprocal lattice vectors have identical values of G_x, therefore all p_x's are distinct. The number of distinct surface wave components dictates the number of equations in the boundary condition. The consequence is that for an ordinary Miller-indexed surface (*i.e.* a periodic surface), the number of boundary equations is $2N/M$ whereas the number is $2N$ for a quasi-periodic surface. The number of equations always matches the number of unknowns, namely, transmission amplitude t_i and reflection amplitude r_j. Each reflection mode has the form of $\exp[ip_x(\mathbf{G})x + ip_y(\mathbf{G})y]$, where

$$p_y(\mathbf{G}) = \sqrt{\omega^2/c^2 - p_x(\mathbf{G})} \qquad (6)$$

Note that there are multiple reflection orders, include evanescent modes on the free space side of the surface. The total number of reflection modes is N/M for a periodic surface and N for a quasi-periodic surface. The reduction of reflection mode for a periodic surface is due to the coincidence of $p_x(\mathbf{G})$ as discussed above (more details are given in the Appendix and Ref. 15).

The above procedures are equally applicable to the refraction problem where a photonic crystal eigenmode impinges on the surface from inside the photonic crystal.

In addition, the transmission of a Gaussian beam or other realistic beam profiles has been analytically calculated,[14,15] overcoming the deficiencies of many existing theories that only address planar incident waves with infinite beam widths. It is shown that the continuity of surface normal component of the Poynting vector results in the conservation of the integrated total power along the beam cross-section. Note that such cross-sections for the incident, reflected, and refracted beams can have any orientation with respect to the surface as shown in Fig. 6. Based on this relation, the insertion loss formulae have been rigorously derived for a Gaussian beam. To our knowledge, all prior analytical studies calculated the value of transmitted optical power based on a planar incident wave with a single wavevector, and then directly used this value for Gaussian beam transmission without justification. Now our work gave it a firm theoretical ground.[15] We note that such derivation is limited to wide beams. The lower limit of the beam width for the above analytic treat of Gaussian beams to be valid is estimated in some cases where the index contrast is relatively small.[34]
With all these issues solved, a complete theoretical framework of the photonic crystal refraction and transmission has thus been established. Figure 6 is taken from our recent paper,[15] which clearly demonstrates the efficiency and accuracy of our modeling method. The calculation based on our method was completed in seconds in contrast to more than 8

hours for the FDTD technique. Note that such an efficient method is essential for modeling the transmission properties of 3D structures, which requires prohibitive computational workload for the FDTD technique.

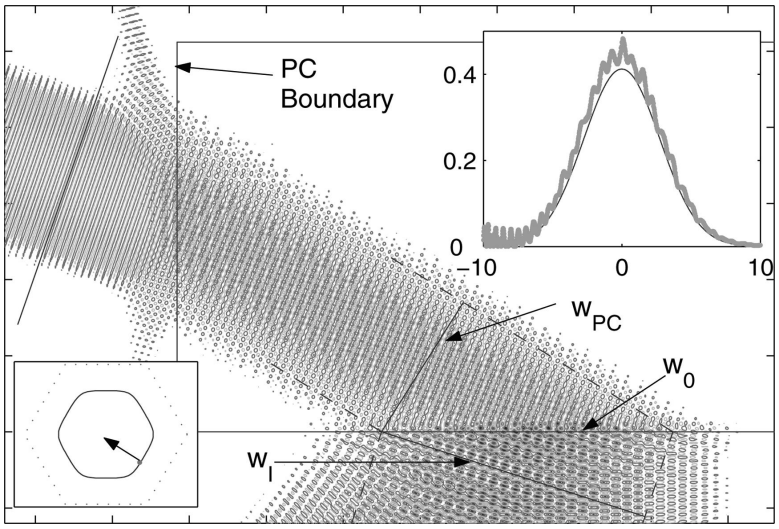

Figure 6 Accurate, efficient theoretical method for photonic crystal refraction. Light impinges upon a rectangular block of photonic crystal from the lower surface, refracts negatively to the left, and exits the left vertical surface. A screen is placed normal to the exiting beam. The beam profiles on the screen obtained from FDTD and our method are displayed in the top inset (vertical axis, relative intensity; bottom axis, lateral distance in microns), The inset shows that our result (thick, green) is in excellent agreement with the FDTD result (thin, dark). Our method achieves same or better accuracies at two to three orders of magnitudes less computational time compared to the FDTD technique. Bottom inset shows the dispersion surface.

4. DEMULTIPLEXER DESIGN

WDM demultiplexers are among the most important applications of photonic crystals. We have applied our theory to design a high channel-count dense WDM demultiplexer and achieved 3dB or lower losses. We calculate the insertion losses for a demultiplexer assuming the exit surface has an angle of 0 degree, 30 degrees, and 60 degrees with respect to the entrance surface. Generally, we find the *total* transmission will be enhanced if the exit surface is perpendicular to the beam in PC. For this reason, one may be tempted to use a polygon with many facets, each facet is approximately normal to the beam at the specified exit location. One such design is sketched in Fig. 7(a). However, for the 30^o exit surface, there are two exiting beams (not plotted) of comparable strength. These two beams propagate in different directions after exiting the photonic crystal as illustrated in Fig. 7(a). The relative intensity (or normalized optical power flux) for the main branching beam is shown in Fig. 7(c). Obviously, the 30^o exit surface has a significant disadvantage due to this issue. Note that although in principle it is possible to collect the intensity of the two exiting beams and send into one output waveguide, it significantly complicates the design and is almost impossible to implement in practice.

The transmission spectra in Fig. 7(c) suggest that for beam angle $>34^o$ inside the photonic crystal, one should use a 60^o exit surface for higher transmission. Note that at a wavelength about 1.555, the 0^o curve crosses the 60^o curve. At this wavelength, the beam angle is about -34^o. The corresponding demultiplexer design is sketched in Fig. 7(b). This design demonstrates lower than 3dB loss over a 25 nm wavelength span (covering >60 WDM channels if 0.4 nm resolution is possible.). Note that if one uses the 0^o surface for exit beams with beam angles up to 85^o, the lateral dimensions of the photonic crystal will increase 6 times or more. In addition, the transmission reduces to less than 25% for large beam angles (or shorter wavelengths) for the 0^o surface.

The parameters for the design presented in Fig. 7(b) were carefully chosen based on the dispersion surface characteristics. It is not enough to just pick a frequency at which the dispersion surface is strongly isotropic, one must choose proper working points on the dispersion surface and proper incident angle to maximize the wavelength sensitivity. The detailed principle governing dispersion surface engineering will be discussed further in the conference presentation.

There is yet another issue we have not addressed in this paper, that is the surface termination. For example, a (*hk*)=(10) surface that ends at the centers of air holes (the surface halves each hole) will have a different transmission from a (10) surface that ends in the solid dielectric region between two rows of holes (no incomplete air holes on the surface). It is not difficult to calculate the transmission for various terminations, although certain caution is necessary to handle some potential numerical issues properly when the surface does not end at hole centers.[33]

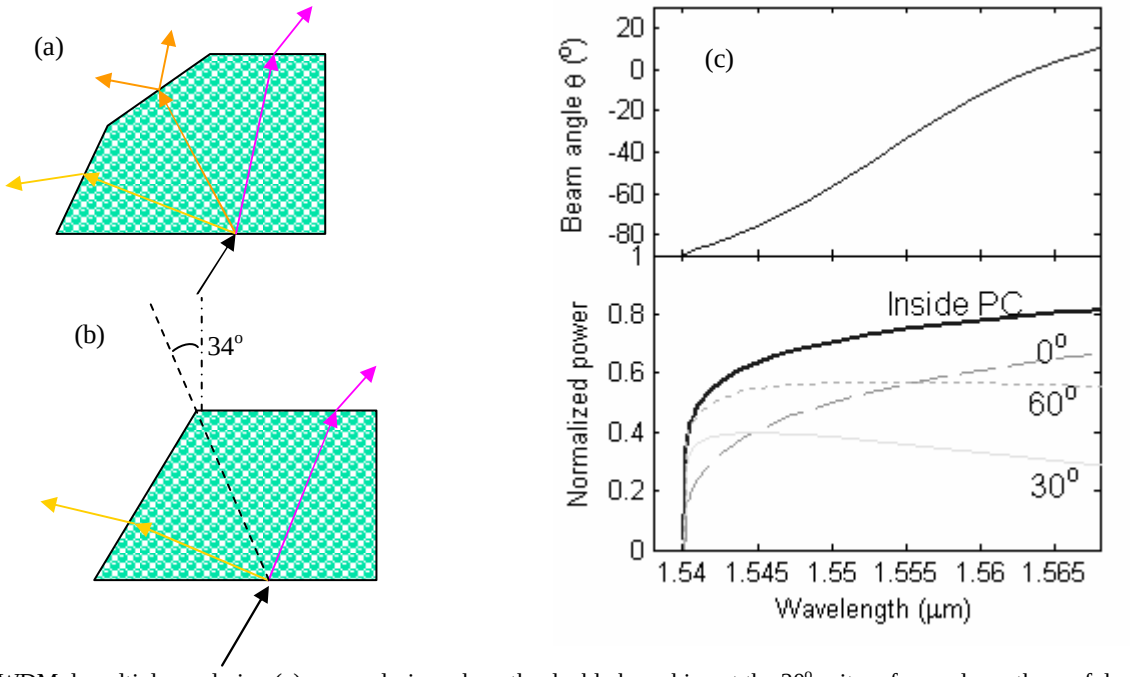

Figure 7 WDM demultiplexer design (a) a poor design where the double branching at the 30° exit surface reduces the useful optical transmission; (b) a good design; (c) Beam angle and transmission vs wavelength for the demultiplexer designs.

5. ULTRA-COMPACT, POWER-EFFICIENT PHOTNIC CRYSTAL WAVEGUIDE MODULATOR

Due to the unique properties of photonic crystals, the size of many optical components is anticipated to be greatly reduced by employing PC structures, such as photonic crystal waveguides. In the most commonly employed configuration, a photonic crystal waveguide is formed by introducing a line defect into a two-dimensional (2D) PC slab. In such PC waveguides, light is confined by a combination of in-plane PBG confinement and vertical index guiding. A size reduction mechanism based on slow group velocity in photonic crystal waveguides has been discussed for an array of optical devices. Notomi *et al.* firstly demonstrated low group velocity and high group velocity dispersion using silicon PC slab line defect waveguides.[5] The extraordinary dispersion of photonic crystal waveguides offers an unprecedented opportunity for developing ultra-compact MZI modulators. As theoretically explained by Soljacic et al., for a fixed frequency of light, the propagation constant $\Delta\beta_{PC}$ of PC waveguide changes as $\Delta\beta_{PC} = \frac{d\beta_{PC}}{d\omega}\Delta\omega_0$, which grows significantly whenever the group velocity $d\omega/d\beta_{PC}$ approaches zero.[35] Such an extraordinary growth of $\Delta\beta_{PC}$ directly leads to a significant enhancement of phase modulation efficiency because the phase change is related to the change of propagation constant and waveguide length L as $\Delta\phi_{PC} = \Delta\beta_{PC} \times L$. One can easily enhance $\Delta\beta_{PC}$ by more than 100 times using a photonic crystal waveguide. Therefore, a 100 times shorter PC waveguide can produce the same phase change as a long conventional waveguide.

Silicon has been the optimal material for microelectronics for a long time, but it has only relatively recently been considered as an option for photonics.[36] Most silicon electro-optic modulators are based on plasma dispersion effect,[37] through which carrier concentration perturbation results in refractive index change. For broadband optical intensity modulators, the silicon Mach-Zehnder Interferometer (MZI) structure that converts a phase modulation into an intensity modulation is widely used. However, conventional silicon MZI modulators are based on rib waveguides, which usually need half to several millimeters to achieve the required phase shift in MZI structures.[38] Here we report a silicon Mach-Zehnder modulator that exploits the slow group velocity in silicon PCWs to reduce the interaction length by two orders of magnitude. A sketch of the device is shown in Fig. 8(a), and the modulation characteristic is shown in Fig. 8(b). Details of this device will be reported elsewhere.

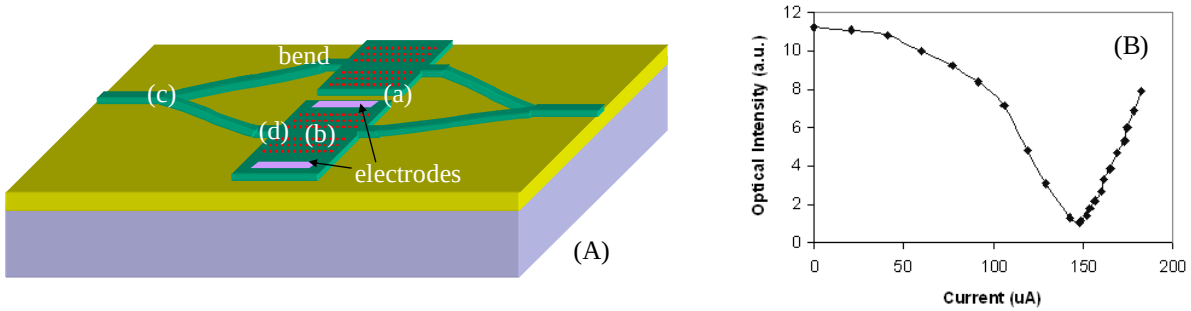

Figure 8 silicon photonic crystal waveguide Mach-Zehnder modulator (A) Schematic of the structure we fabricated on an silicon-on-insulator chip. Green layer—silicon, yellow layer—SiO_2, (a) PCW active/functional region, (b) PCW, (c) y-junction. (B) Transmitted optical intensity versus injection current. Over 90% modulation depth was achieved at 0.15mA peak current with 80 micron long photonic crystal waveguides.

ACKNOWLEDGEMENTS

This work is supported in part by AFRL, and AFOSR. The authors thank the State of Texas and SEMATECH for support under the AMRC program. Nanofabrication facilities at UT MRC are partially supported by NSF's NNIN program. We thank the CNM of UT Austin, Welch Foundation and SPRING for the Dual Beam FIB/SEM usage.

REFERENCES

1. E. Yablonovitch, *Phys. Rev. Lett.*, vol. 58, 1059,(1987).
2. S. John, *Phys. Rev. Lett*., vol. 58, 12486 (1987).
3. O. Painter, R. K. Lee, A. Scherer, A. Yariv, J. D. O'Brien, D. P. Dapkus, I. Kim, "Two-dimensional photonic band-gap defect lasers," Science, vol. 284, pp. 1819 (1999).
4. A. Mekis, J. C. Chen, I. Kurland, S. Fan, P. R. Villeneuve, J. D. Joannopoulos, "High transmission through sharp bends in photonic crystal waveguides," Phys. Rev. Lett., vol.77, 3787, 1996.
5. M. Notomi, K. Yamada, A. Shinya, J. Takahashi, C. Takahashi, and I. Yokohama, "Extremely Large Group-Velocity Dispersion of Line-defect Waveguides in Photonic Crystal Slabs," Physical Review Letters, vol. 87, 253902 (2001).
6. W. Jiang and R. T. Chen, "Multichannel optical add-drop process in symmetrical waveguide-resonator systems," *Phys. Rev. Lett.*, vol. 91, pp. 213901 (2003).
7. W. Jiang *et. al.* "Theoretical and experimental study of photonic-crystal-based structures for optical communication applications," Photonics West, San Jose, January 2004, Proc. SPIE, vol. 5360, pp. 190-198 (2004).
8. H. Kosaka, et. al., Phys. Rev. B, vol. 58, 10096 (1998).
9. H. Kosaka, et al. J. Lightwave Technol. Vol. 17, 2032 (1999).
10. L. Wu, M. Mazilu, T. Karle, and T. F. Krauss, J. Quant. Electron. Vol. 38, 915 (2002).
11. C. Luo, S. G. Johnson, J. D. Joannopoulos, Phys. Rev. B, vol. 65, 201104 (2002).
12. T. Baba and M. Nakamura, J. Quantum Electron., vol. 38, 909 (2002).
13. T. Baba and T. Matsumoto, Appl. Phys. Lett. vol. 81, 2325 (2002).
14. W. Jiang *et. al.* "Superprism effect and light refraction and propagation in photonic crystals," Proc. SPIE, vol. 5733 pp. 50-57 (2005).
15. W. Jiang, R. T. Chen, X. Lu, "Theory of light refraction at the surface of a photonic crystal," Phys. Rev. B 71, 245115 (2005).
16. J. B. Pendry and A. MacKinnon, Phys. Rev. Lett. vol. 69, 2772 (1992).
17. T. Minami, H. Ajiki, and K. Cho, Physica E vol. 13, 432 (2002).
18. Z. Li and K. Ho, Phys. Rev. B vol. 68, 155101 (2003).
19. K. Ohtaka, T. Ueta, and K. Amemiya, Phys. Rev. B vol. 57, 2550 (1998).
20. N. Stefanou, V. Yannopapas, and A. Modinos,Comput. Phys. Commun., vol, 132, 189 (2000).
21. T. Ochiai and J. Sanchez-Dehesa, Phys. Rev. B, vol. 64, 245113 (2001).
22. J. Bravo-Abad, T. Ochiai, and J. Sanchez-Dehesa, Phys. Rev. B vol. 67, 115116 (2003) and references therein.
23. K. Sakoda, Phys. Rev. B, vol. 52, 8992 (1995).
24. K. B. Chung and S. W. Hong, Appl. Phys. Lett. vol. 81, 1549 (2002).

25. D. Felbacq and R. Smaali, Phys. Rev. Lett. 92, 193902 (2004).
26. J. S. Zhu, X. M. Lu, Wei Jiang, W. Tian, Y. N. Wang, J. Appl. Phys, vol. 81, pp. 1392 (1997).
27. L. Li, J. Opt. Soc. Am. A vol. 13, 1024 (1996).
28. L. C. Botten, N. A. Nicorovici, R. C. McPhedran, C. Martijn de Sterke, and A. A. Asatryan, Phys. Rev. E, vol. 64, 46603 (2001).
29. J. E. Dennis, J. F. Traub, and R. P. Weber, SIAM J. Numer. Anal. Vol 13, 831 (1976), and references therein.
30. P. Lancaster, *Lambda-matrices and Vibrating Systems*, (Pergamon, Oxford, 1966).
31. A. L. Mackay, Physica A, vol. 114, 609 (1982).
32. Notomi, M.; Suzuki, H.; Tamamura, T.; Edagawa, K.; Physical Review Letters, vol.92, 123906 (2004).
33. Wei Jiang, PhD dissertation, the University of Texas at Austin, 2005 (completed in December 2004).
34. W. Jiang, C. Tian, R. T. Chen, unpublished, 2003.
35. M. Soljacic, S. G. Johnson, S. Fan, M. Ibanescu, E. Ippen, and J. D. Joannopoulos, J. Opt. Soc. Am. B 19, 2052 (2005); M. Soljacic, J.D. Joannopoulos , *Nature materials*, vol. 3, pp. 211-219, 2004.
36. R. A. Soref, B. R. Bennett, "Electrooptical effects in silicon," *IEEE J. Quantum Electron.* QE-23, 123-129 (1987)
37. R. A. Soref, *Proceeding of SPIE*, vol. 5730, pp. 19 – 28, (2005).
38. A. Liu, R. Jones, L. Liao, D. Samara-Rubio, D. Rubin, O. Cohen, R. Nicolaescu, and M. Paniccia, Nature 427, 615-618 (2004).

APPENDIX: MATHEMATICAL DETAILS FOR PHOTONIC CRYSTAL REFRACTION

Consider a lossless periodic dielectric medium (or a photonic crystal) being cut along an arbitrary direction to form a semi-infinite medium that fills the half space $y>0$. A planar wave with infinite beam extent in the xz-plane is incident on the semi-infinite medium surface. The circular frequency $\omega=2\pi c/\lambda$, and lateral wave vector components k_x and k_z of the monochromatic planar wave are given.

Theorem 1 For any given values of ω, k_x and k_z, the solved eigenmodes of the time-independent Maxwell's equation can always be partitioned into two groups. The first group contains those propagating modes whose energy flow as specified by Poynting vector or group velocity points toward $+y$ direction and those evanescent modes whose intensity decays as $y\rightarrow\infty$. The second group contains those propagating modes whose energy flow points toward $-y$ direction and those evanescent modes whose intensity decays as $y\rightarrow-\infty$.

Theorem 2 For any given values of ω, k_x and k_z, and any given surface orientation with respect to the principle axes of the photonic crystal, the surface-dependent degeneracy of the solved eigenmodes and the coincidence of the surface-parallel components of the reciprocal lattice vectors are always correlated such that the number of equations and number of unknowns always match in solving the boundary conditions on the surface of the semi-infinite crystal.

Corollary For the boundary conditions of an arbitrary periodic surface, generally a proper set of linear equations can be constructed only by redefining the lattice basis vectors in certain manners such that a surface-normal 1D Brillouin zone is explicitly identified.

We would like to add some comments about these theorems. In Theorem 2, the coincidence of the surface-parallel components of the reciprocal lattice vectors **G** refers to the projection of the any **G** on the xz-plane. As we have seen in Eq. (5) for a 2D case, if two different **G**'s have the same x component, then they give identical surface wave vector $p_x(\mathbf{G})$ and contribute to a single surface wave component. Note the number of distinct surface wave vectors directly dictates the number of independent equations in the boundary conditions. The proofs can be found in Refs. 15 and 33.

For surfaces like $(hk)=(23)$ or indexed by larger integer values, the basis vectors of lattice need to be redefined to reflect the surface orientation. The way of redefining the lattice basis vectors mentioned in the preceding Corollary is given in Eq. (5) for a 2D case of Ref. 15, and that can be easily generalized to any 3D case with two independent lattice vector on a surface in 3D. The dotted red parallelogram in Fig. 9(b) represents the first BZ corresponding to the redefined basis vectors. However, in some sense, any 2D Brillouin zone of the original lattice is no longer meaningful for a semi-infinite crystal. The presence of the surface breaks the 2D discrete translational symmetry. If the surface can be represented by integer or Miller indices, then one can show that the semi-infinite crystal still has 1D translational symmetry in the direction parallel to the surface. In this case, such 1D discrete translational symmetry leads to 1D periodicity in the surface normal direction in the reciprocal space. For a 2D photonic crystal with x, y axes established as in Fig. 4(a), the 1D periodicity along x-axis in real space results in 1D periodicity along y-axis in reciprocal space. Because of such 1D periodicity in reciprocal space, one can define 1D Brillouin zones for a semi-infinite photonic

crystal. The k_y eigenvalues must be restricted to one of the 1D Brillouin zones. It can be readily proved that for a Fourier expansion that includes M components in the surface normal direction, all eigenvalues of k_y outside one such Brillouin zone give M replicas of the eigenmode fields of those inside.[15] To reduce such degeneracy, one must restrict to those modes inside one 1D Brillouin zone.

Figure 9 illustrates the concept of surface-dependent mode degeneracy in three cases. There is one dot on each branch of dispersion surface. Each dot represents the equivalent eigenmode in the corresponding BZ. In Fig. 9(a), the degree of degeneracy is easily identified to be 5 for 5x5 Brillouin zones. However, once the surface orientation changes to (23), the degree of degeneracy for 5x5 BZs becomes questionable. Figure 9(b) suggests a degree of degeneracy 2. However, any attempt to solve the boundary conditions based on this value will fail unless we first redefine the basis vectors of the lattice to adapt to the surface orientation. The rule for redefining the basis vectors is given in Ref. 15. One proper Brillouin zone based on the redefined lattice vectors has the parallelogram shape as indicated by red dotted lines in Fig. 9(b). Although a 2D Brillouin zone is drawn, only its vertical edge on the constant k_x line (*i.e.* the 1D BZ) is relevant for the mode degeneracy. The modes repeated in reciprocal space along the other new reciprocal lattice vector are not on the constant k_x line, therefore are not the permitted solution for the refraction problem. Also, for the newly defined lattice unit cell, the reciprocal cell may be reduced in size, and therefore the dispersion contours may multiply its density in the size-reduced new BZ. This effect is automatically addressed in our analytic treatment that follows redefining the lattice unit cell.[15,33] Lastly, a quasi-periodic surface is shown in Figure 9(c). Note the cross-section of the holes on the surface never repeats, *i.e.* has no periodicity. Correspondingly, in the reciprocal lattice, the constant k_x line never crosses the equivalent point in different branches of the dispersion surface in the different BZs. In all cases, one can see that the surface periodicity in real space is correlated to the periodicity of reciprocal space in the surface-normal direction. Compare Fig. 9(a) and 9(c), one readily recognize that a slight variation of surface orientation that changes a surface from periodic to quasi-periodic. In the reciprocal space, this causes one refracted beam to split into essentially infinite number of beams whose energy flow points to distinct directions as indicated by the arrows in Fig. 9(c). In fact, the orientation of a surface can be described by the angle φ of surface normal with respect to one of the crystal axes. It can be shown that the φ values for a periodic and a quasi-periodic surface are inter-dispersed in a similar fashion that rational and irrational numbers are intermixed on the real axis.

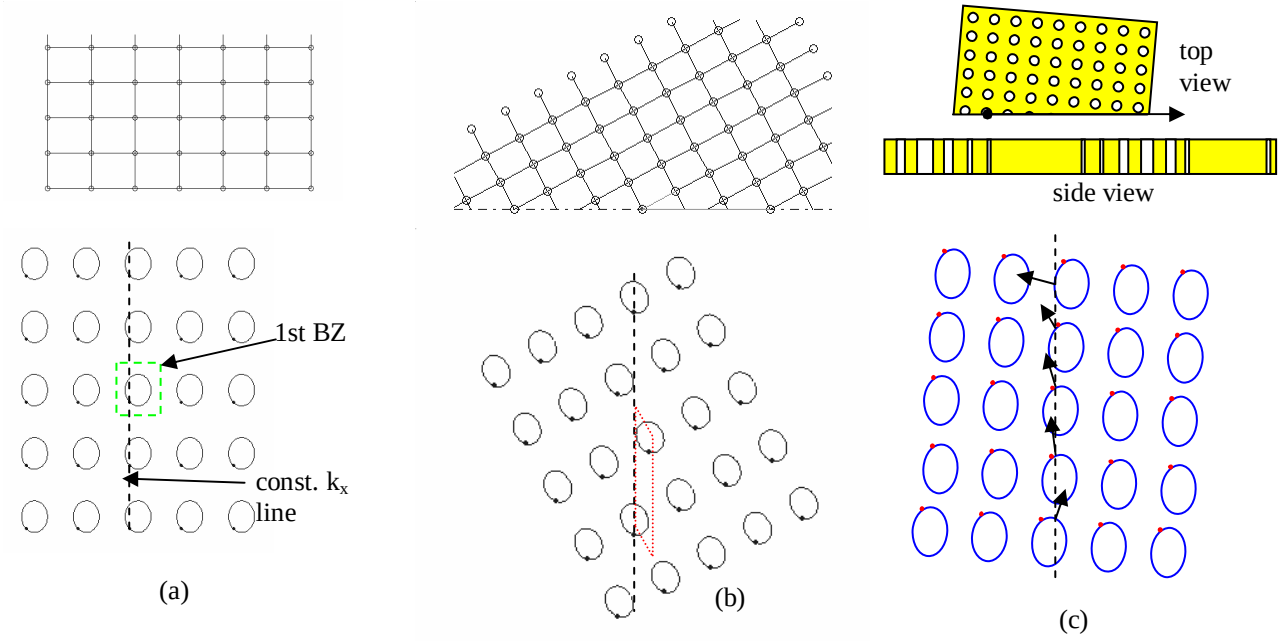

Figure 9 Various surface orientations for a 2D rectangular lattice and the surface-dependent mode degeneracy. For each case, the upper diagram shows the lattice with surface located at the bottom, the lower diagram shows the dispersion surface of a given frequency. (a) Miller indices (*hk*)=(10); (b) Miller indices (*hk*)=(23); (c) Quasi-periodic surface that cannot be described by integer (or rational-numbered) Miller indices. The cross-section of the holes on the surface has no periodic pattern as can be seen from the side view.